THE MECHANICS OF INSTABILITY-LINE FORMATION

By Donald C. House

United States Weather Bureau Severe Local Storms Forecast Center, Kansas City[1]

(Manuscript received 19 May 1958)

ABSTRACT

It is proposed that under certain conditions of wind flow that temperature changes due to horizontal advection and vertical motion produce a trend towards the formation within a few hours of a line or narrow band of vertical thermal instability associated with a marked increase in low-level convergence along the same line or narrow band.

An assumed distribution of winds, chosen to represent typical conditions observed preceding by a few hours the formation of an instability line, is studied and a model presented. The model agrees well with synoptic observation and studies. The atmospheric mechanism derived is of the mesoscale and is directly applicable to instability line formation in the "High Plains" and most pre-cold frontal instability lines in other areas can be explained by it.

1. Introduction

A paper by Fulks [5], "The instability line," discussed the problems of formation and forecasting of the instability line.[2] Since that paper was published, more emphasis in this country has been placed on the forecasting of severe-weather types (severe thunderstorms, hail, and tornadoes) normally associated with such lines.

Fulks points out that low-level convergence is a necessity along the instability line and needs to be explained in terms of other factors. He raises the question, "Are there other factors which first act to produce low-level horizontal convergence and upper-level divergence, or is vertical motion merely the result of vertical instability and thus the full cause of the convergence-divergence pattern?"

Based upon experience gained as a result of concentration upon the problem of forecasting severe local storms, it is the consensus of the Weather Bureau's severe local-storm forecasters that there are broad-scale factors that first act to produce upper-level horizontal divergence and low-level horizontal convergence in most instances of pre-cold-frontal instability-line formation.

The purpose of this paper is to demonstrate a physical process which can produce a decrease in thermal stability in the same area that an increase in positive vertical motion occurs. The results agree rather closely with what is observed in synoptic practice.

[1] Presented at 150th National Meeting of the American Meteorological Society, 28–31 January 1957; ms. revised December 1957.

[2] The non-frontal squall line has been designated by the World Meteorological Organization as the "instability line." It is a line of incipient, active, or dissipating non-frontal instability conditions. It is an analytical tool for indicating, primarily, the incipient and dissipating stage of squall-line phenomena.

2. The hypothesis

Inherent in a typical wind and temperature field existing a few hours prior to the formation of an instability line, there is a pattern of vertical motion, horizontal temperature advection, and low-level insolational heating causing a marked decrease of thermal stability in a restricted area or along a narrow band within a relatively short time.

To show this, an upper-level wind field typical (as far as our observational network can inform us) of those just prior to instability-line formation was selected (fig. 1). These fields, chosen on the basis of experience, agree approximately with the composite charts prepared by Beebe [1] for his areas II and III. A vertical-temperature curve is also chosen to represent initial conditions in the approximate position where the instability line later forms (fig. 2). Initial conditions are also chosen such that there is no horizontal temperature gradient at the 1000-mb surface and this surface is at mean sea level. Further, a rate of surface pressure change (fig. 3) is assumed at the initial time representing that due to mass divergence. All computations are made by finite differences and interpolation between levels. Further assumptions are:

1. That initially the process takes place at a time of the day when insolational heating at low levels is effective.
2. There is no release of latent heat of condensation, and therefore the process applies only up to the time that condensation begins.
3. The process is adiabatic except for a reasonable assumed rate of daytime warming in the low levels.

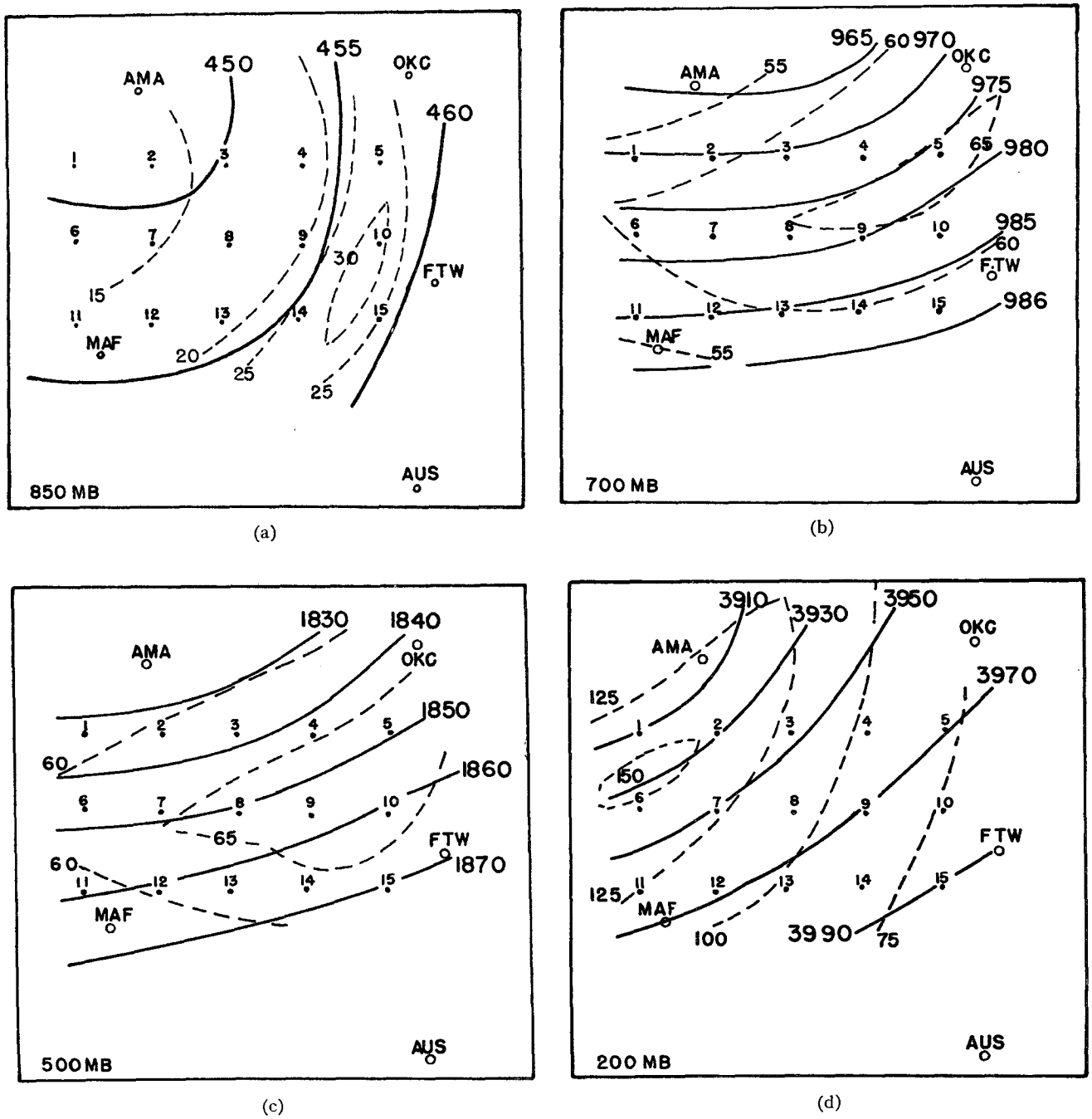

FIG. 1. Contours (heavy solid lines contour height values in 10's of feet) and isotachs (dashed lines) assumed at initial time at 850-mb (fig. 1a), 700-mb (fig. 1b), 500-mb (fig. 1c) and 200-mb (fig. 1d) levels. The serially numbered points indicate the location of the grid points referred to in the text. This grid is fixed for all subsequent figures.

3. The model

In the development of the model, all computations will be made at the grid points shown on the various charts on which points are numbered for reference purposes.

Figs. 1a to 1d show the assumed initial wind field and the computed contour fields at the 850-, 700-, 500-, and 200-mb surfaces. Fig. 2 shows the assumed initial-temperature sounding over grid point 9 chosen as typical of conditions in the area of formation of an instability line some few hours prior to its formation. The contour patterns at the several pressure levels were computed as follows:

1. The initial heights of the 850-, 700-, 500-, and 200-mb surfaces (height of 1000-mb surface assumed zero), were computed for point 9 on the basis of the assumed initial sounding and hydrostatic considerations.

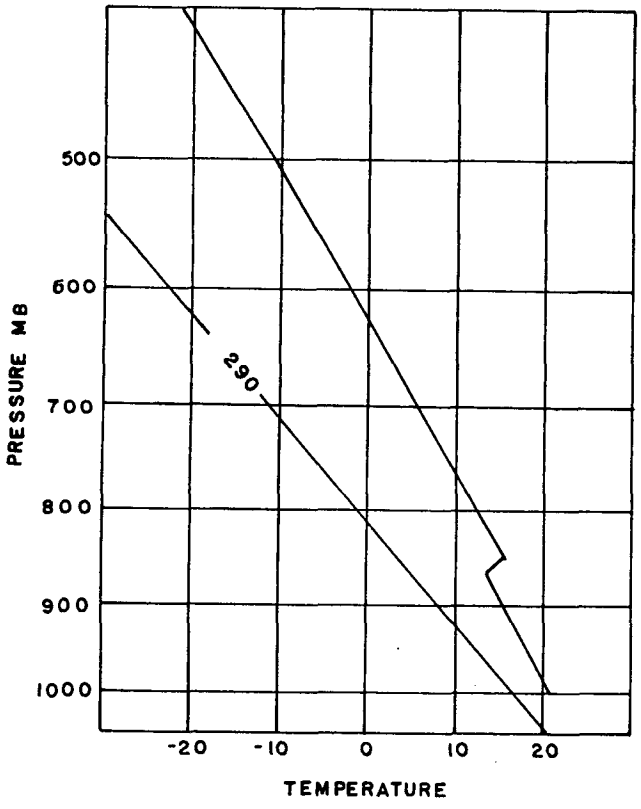

FIG. 2. Temperature sounding over point 9 assumed at initial time.

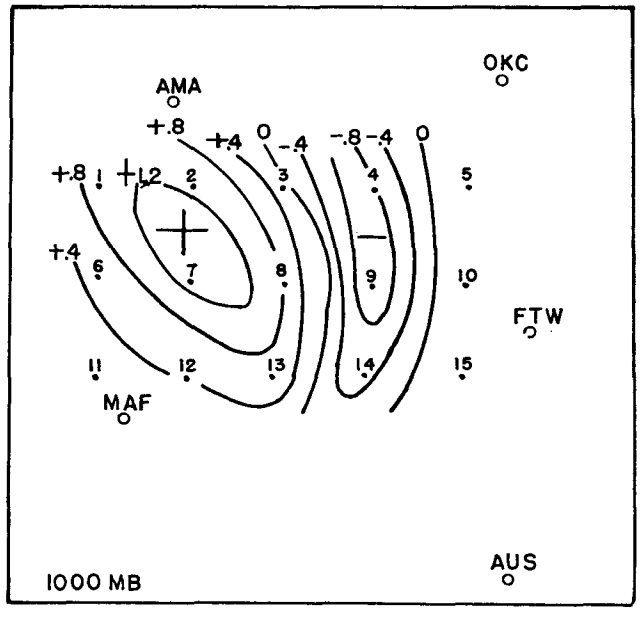

FIG. 3. Rate of surface-pressure change in millibars per 3 hr assumed at initial time.

2. By taking the wind fields at the several constant-pressure surfaces and applying the gradient-wind equation (with the assumption that the radius of curvature of the trajectory of the air parcel equals the radius of curvature of the streamlines which in turn is equal to that of the contours) the contour gradients were determined.

The remaining initial-temperature soundings for the numbered points of the grid were constructed by interpolation of the thickness of the layers over the points, establishing the mean virtual temperature for the layers and assuming the mean virtual temperature of the layer to be the same as the temperature at the mid-point of the layer. Determination of the mean virtual temperature of the several layers over the grid points permits the construction of the temperature soundings that are hydrostatically consistent with the assumed initial conditions.

Temperature soundings at the initial time for points 6, 7, 8, 9, and 10 are shown in figs. 9a through 9e. The temperature inversion at point 9 was arbitrarily prescribed. The temperature inversions at points 6, 7, 8, and 10 result from thickness considerations for the layers 1000 to 850 mb and 850 to 700 mb. Initial conditions were chosen such that the 1000-mb temperatures for all grid points are equal. Thickness considerations in the lower level indicate a constant decrease of temperature with height through the layer. In the layer 850 to 700 mb, thickness considerations require that the temperature curves be either isothermal or that an inversion be introduced. An isothermal lapse rate of such vertical extent is not normally observed in such synoptic patterns. Therefore the magnitude of the inversions and their vertical position were determined consistent with thickness requirements, the result being a marked similarity to the assumed initial sounding over point 9.

Temperature changes were determined by consideration of the following equation:

$$\frac{\partial T}{\partial t} = \frac{1}{c_p}\frac{dQ}{dt} - \mathbf{V}\cdot\nabla_2 T - w(\gamma_d - \gamma) \qquad (1)$$

where Q is heat in calories, T is temperature, γ_d is dry adiabatic lapse rate, γ is actual lapse rate and w is vertical velocity. The first term on the right gives the effect of heat added to the system (here we will consider only the effect of diurnal heating in the low-levels); the second term gives the effect of horizontal temperature advection and the third term the temperature change due to vertical motion.

For the first term on the right-hand side, it was assumed that warming occurred at the rate of 1.5C per hr at the ground level and that this amount of warming produced a dry adiabatic lapse rate up to the intersection of the dry adiabat with the temperature curve as otherwise determined. For all higher levels, the effect of this term was assumed zero.

Initial values of the term $\mathbf{V}\cdot\nabla_2 T$ were computed from the following equation (see, for example,

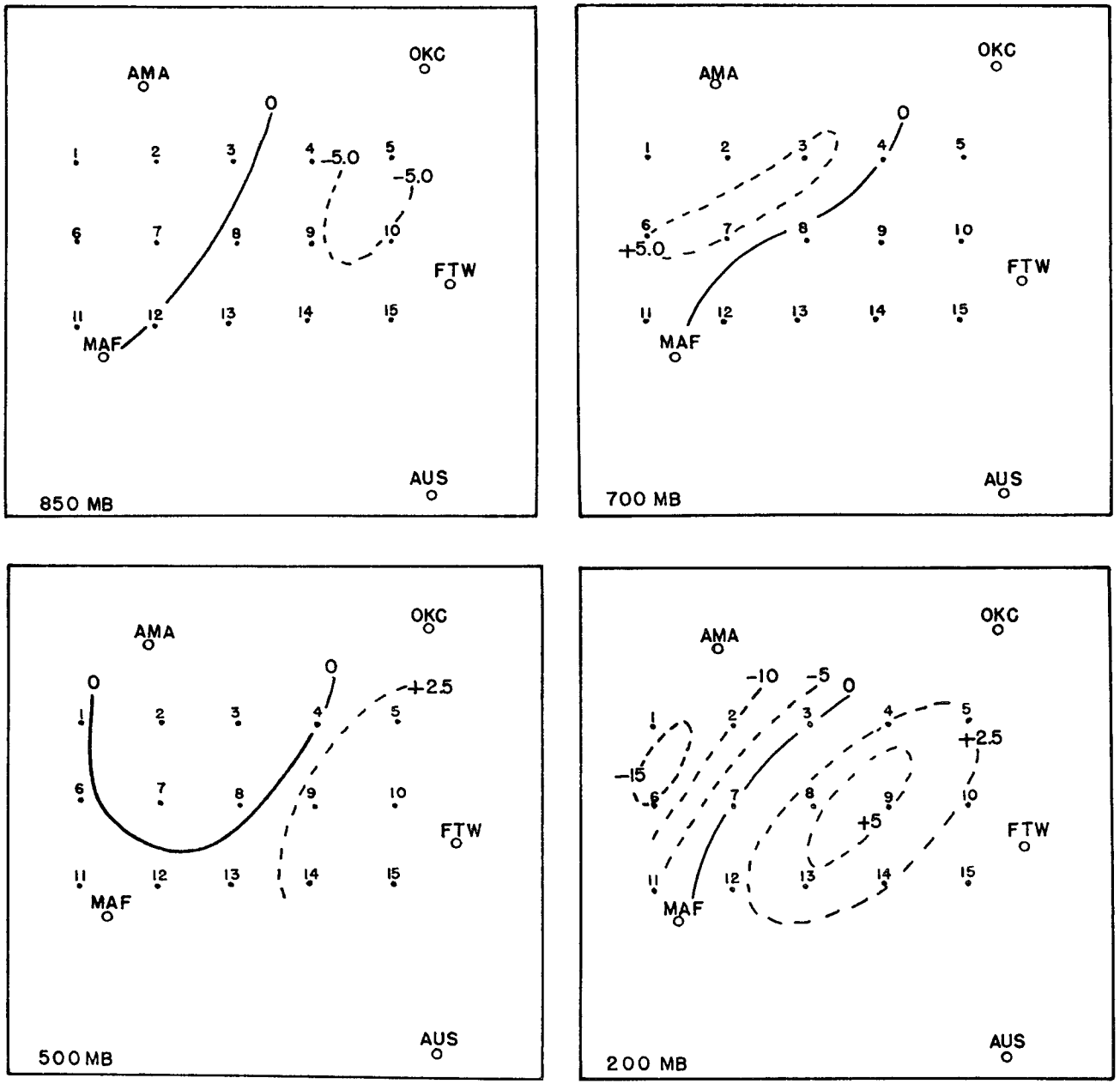

FIG. 4. Distribution of $\text{div}_2 \mathbf{V}$ of fig. 1 (initial time) at levels indicated in units of 10^{-5} sec^{-1}. Positive values: divergence; negative values: convergence.

Panofsky [9] p. 102):

$$\mathbf{V} \cdot \nabla_2 T = V^2 \left(\frac{\partial \alpha}{\partial z} \right) \frac{fT\pi}{g \times 180}, \qquad (2)^3$$

where

V = wind speed,
$\partial\alpha/\partial z$ is the turning of wind direction with height, positive clockwise,
f = Coriolis parameter,
T = temperature,
g = acceleration of gravity,

in which the wind is assumed to be geostrophic.

[3] Equation (2) is derived for an infinitesimally thin layer and its extension for use with a discrete layer *may* introduce considerable error in determination of advective rates when:

1. Values of $\partial\alpha/\partial z$ are large, and
2. The difference between V at the bottom and top of the layer is large.

The error in applying the equation here has introduced a maximum error of 0.3C in the mean temperature of any column or a height error of about 40 ft at the 200-mb level at the end of the second time step. For the purpose of this study, such an error does not appear to be critical with the net effect being a slight increase in gradient at the lowest levels and a slight decrease in gradient at the 200-mb level.

TABLE 1. Computed temperature changes due to horizontal advection and vertical motion over numbered grid points, at level indicated, during the first time step.

	Level	2.25 km		4.25 km		8.75 km	
		$-\mathbf{V}\cdot\nabla^2 T$	$-w(\gamma_d-\gamma)$	$-\mathbf{V}\cdot\nabla^2 T$	$-w(\gamma_d-\gamma)$	$-\mathbf{V}\cdot\nabla^2 T$	$-w(\gamma_d-\gamma)$
Grid point	1	−0.5	+1.4	−0.1	+3.0	−5.2	+2.7
	2	0.0	+1.1	−0.9	+2.9	−4.3	+1.8
	3	+1.8	+0.6	−1.0	+1.9	−2.8	+0.7
	4	+3.0	0.0	−0.3	0.0	−1.4	0.0
	5	+3.5	0.0	0.0	0.0	0.0	0.0
	6	−0.2	+1.4	−0.2	+2.2	−4.3	+2.7
	7	0.0	+1.2	−0.8	−0.8	−3.5	−0.2
	8	+1.1	+0.5	−0.7	−0.1	−1.7	−0.3
	9	+2.6	0.0	+0.1	0.0	−1.0	0.0
	10	+3.1	0.0	−0.2	0.0	−0.4	0.0
	11	0.0	+0.3	−0.4	+0.4	−1.3	+0.7
	12	+0.1	0.0	−0.7	0.0	−0.8	0.0
	13	+1.2	−0.2	−1.9	−0.5	−0.7	0.0
	14	+1.9	−0.3	−0.6	−0.5	−0.5	0.0
	15	+2.6	0.0	−0.3	0.0	−0.4	0.0

Computations of $\mathbf{V}\cdot\nabla_2 T$ were made for each layer 850 to 700 mb, 700 to 500 mb, and 500 to 200 mb. T was taken as the mean temperature of the layer and no distinction was made for this purpose between actual and virtual temperature. V was taken as the mean geostrophic wind of the layer. The computed initial values of $\mathbf{V}\cdot\nabla_2 T$ are tabulated in deg C per hour in table 1 for the approximate mid-level of each layer and for each of the grid points.

In order to compute w, the vertical motion, the horizontal-velocity divergence was first computed for each level by the following equation (see, for example, Panofsky [9] p. 35):

$$\mathrm{div}_2\,\mathbf{V} = \frac{\partial V}{\partial S} + \frac{V\pi}{180}\frac{\partial \alpha}{\partial n}, \tag{3}$$

where

V is wind speed,

α is wind direction in degrees increasing clockwise from north,

s is coordinate parallel to streamline and positive in direction of wind,

n is coordinate normal to streamline and directed to the right of the wind.

The terms $\partial V/\partial S$ and $\partial\alpha/\partial n$ were evaluated by finite differences using the system of grid points shown. Grid points are separated by a distance equal to one degree of latitude; $\partial V/\partial S$ and $\partial\alpha/\partial n$ were computed over that distance. The results are shown in figs. 4a through 4d.

The resulting initial distribution of divergence in the vertical section 6–10 is shown in fig. 5. This chart was drawn by interpolation between the computed values for the various levels.

The initial values of w (vertical velocity) were then computed for each of the grid points and for each km of height using the following approximation:

$$w_2 = \frac{\rho_1}{\rho_2} w_1 - \tfrac{1}{2}\left(\frac{\rho_1}{\rho_2}\mathrm{div}_2\,\mathbf{V}_1 + \mathrm{div}_2\,\mathbf{V}_2\right)(z_2 - z_1), \tag{4}$$

where

w is vertical velocity,
ρ is density,
z is height of layer, and
subscripts 1 and 2 refer to bottom and top of layer, respectively.

The resulting initial distribution of vertical motion for the section 6–10 is shown in fig. 6.

From initial values of w so determined and the initial temperature curves, the initial values of the term $w(\gamma_d - \gamma)$ were computed. These are tabulated in table 1 in deg C per hour for the mid-height of each layer and over each of the grid points.

At this point, a determination has been made of the initial rate of temperature change inherent in the assumed initial wind field and assumed rate of temperature change due to insolation effective in the lowest layer. The conditions producing these changes, *i.e.*, the wind field and addition of heat due to insolation, are considered stationary for 90 min.

By adding to the initial values of mean temperature for the layers 1000 to 850 mb, 850 to 700 mb, 700 to 500 mb, and 500 to 200 mb, the temperature changes occurring as a result of pressure changes, temperature advection, vertical motion and low-level heating, new values of mean temperature and the thicknesses of the several layers were determined at the end of the 90-min time interval. Soundings, consistent with these data, were computed for all grid points and those for points 6, 7, 8, 9, and 10 are shown in figs. 9a through 9e. The magnitudes of the inversions and their vertical position were determined through the relationship of mean temperature and thickness of the several layers.

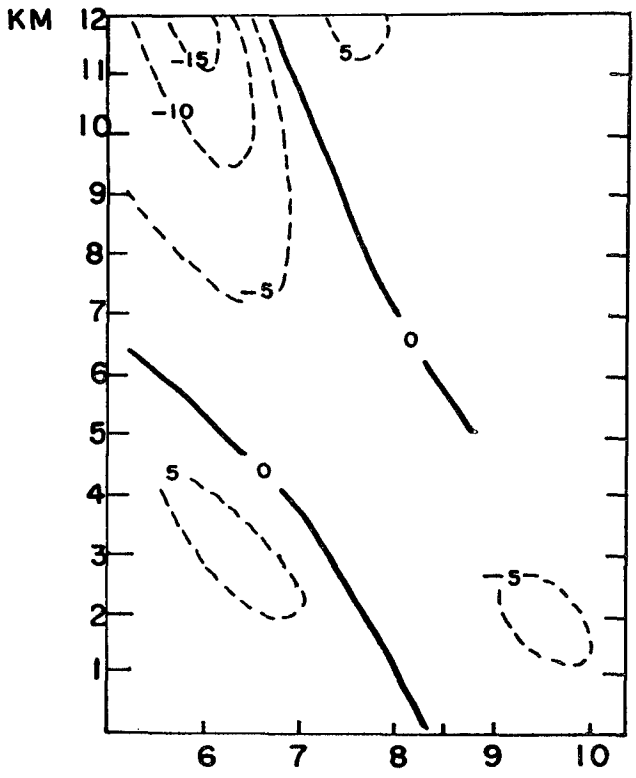

FIG. 5. Vertical distribution of $\text{div}_2 \mathbf{V}$ along section 6–10 at initial time.

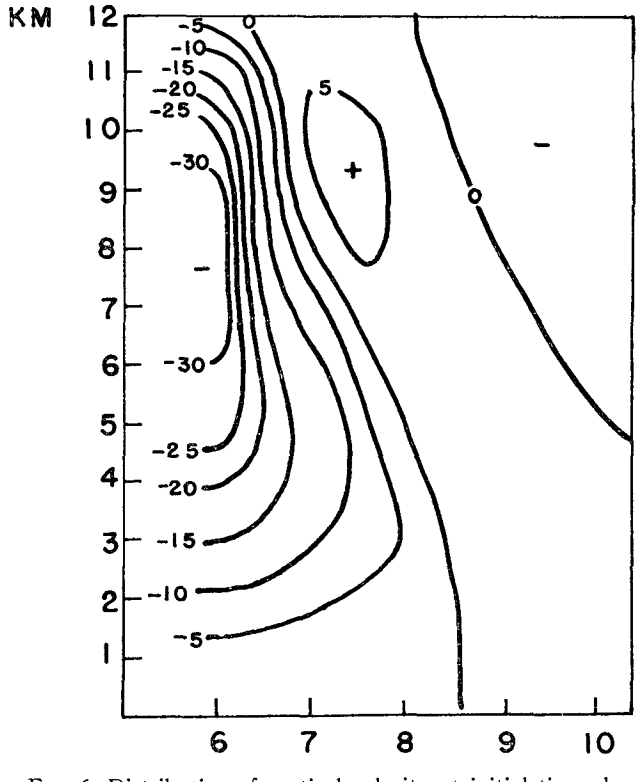

FIG. 6. Distribution of vertical velocity at initial time along section 6–10 computed from distribution of $\text{div}_2 \mathbf{V}$ shown in fig. 5. Units are cm sec^{-1} positive upward and negative downward.

It should be noted that the combination of temperature changes due to vertical motion, advection, and addition of heat due to insolation during this time interval has acted only to maintain or intensify the strength of the inversions without any appreciable vertical displacement. From the thickness values for the various layers over all grid points, new contour fields were determined. From these contour fields, gradient winds were computed to establish the new wind field. The new contour fields and wind speeds are shown in figs. 7a through 7e.

Ideally, the next step would be to recompute the values of $\mathbf{V}\cdot\nabla_2 T$ and $w(\gamma_d - \gamma)$ for all grid points on the basis of the new wind fields and to let the process act for an additional time period. However, an inspection of the new contour pattern reveals the appearance of a sharply defined mesoscale high over point 7 at the 500-mb level with a small radius of curvature to the contours. This suggests that the wind flow at this level in the vicinity of this HIGH may be non-gradient making computations of $\mathbf{V}\cdot\nabla^2 T$ and $w(\gamma_d - \gamma)$ in the layers 700 to 500 mb and 500 to 200 mb in its vicinity unreliable when using the gradient assumption. Therefore, computations of these values were restricted to grid points 4, 5, 9, 10, 14, and 15 supplemented by additional computations at points midway between these numbered grid points. The divergence fields so determined are shown in figs. 8a through 8e.

Following the same procedure as initially, values of $\mathbf{V}\cdot\nabla^2 T$ and $w(\gamma_d - \gamma)$ were obtained for the various layers over grid points 4, 5, 9, 10, 14, and 15 and these values are shown in table 2. These rates of temperature change in addition to that assumed due to the non-

TABLE 2. Computed temperature changes due to horizontal advection and vertical motion over numbered grid points, at level indicated, during the second time step.

	Level	0.75 km		2.25 km		4.25 km		8.75 km	
		$-\mathbf{V}\cdot\nabla^2 T$	$-w(\gamma_d - \gamma)$	$-\mathbf{V}\cdot\nabla^2 T$	$-w(\gamma_d - \gamma)$	$-\mathbf{V}\cdot\nabla^2 T$	$-w(\gamma_d - \gamma)$	$-\mathbf{V}\cdot\nabla^2 T$	$-w(\gamma_d - \gamma)$
Grid Point	4	0.0	−0.2	0.0	−2.0	0.0	−4.3	−2.1	−1.9
	5	+0.2	0.0	+6.4	0.0	+0.5	0.0	−1.4	0.0
	9	0.0	−0.2	0.0	−4.5	−0.0	−3.7	−1.1	−2.5
	10	+0.7	0.0	+3.1	−2.0	+0.7	−0.7	−0.7	0.0
	14	+0.2	0.0	+0.6	0.0	+0.6	0.0	−0.4	0.0
	15	+0.4	0.0	+0.5	0.0	+0.3	0.0	0.0	0.0

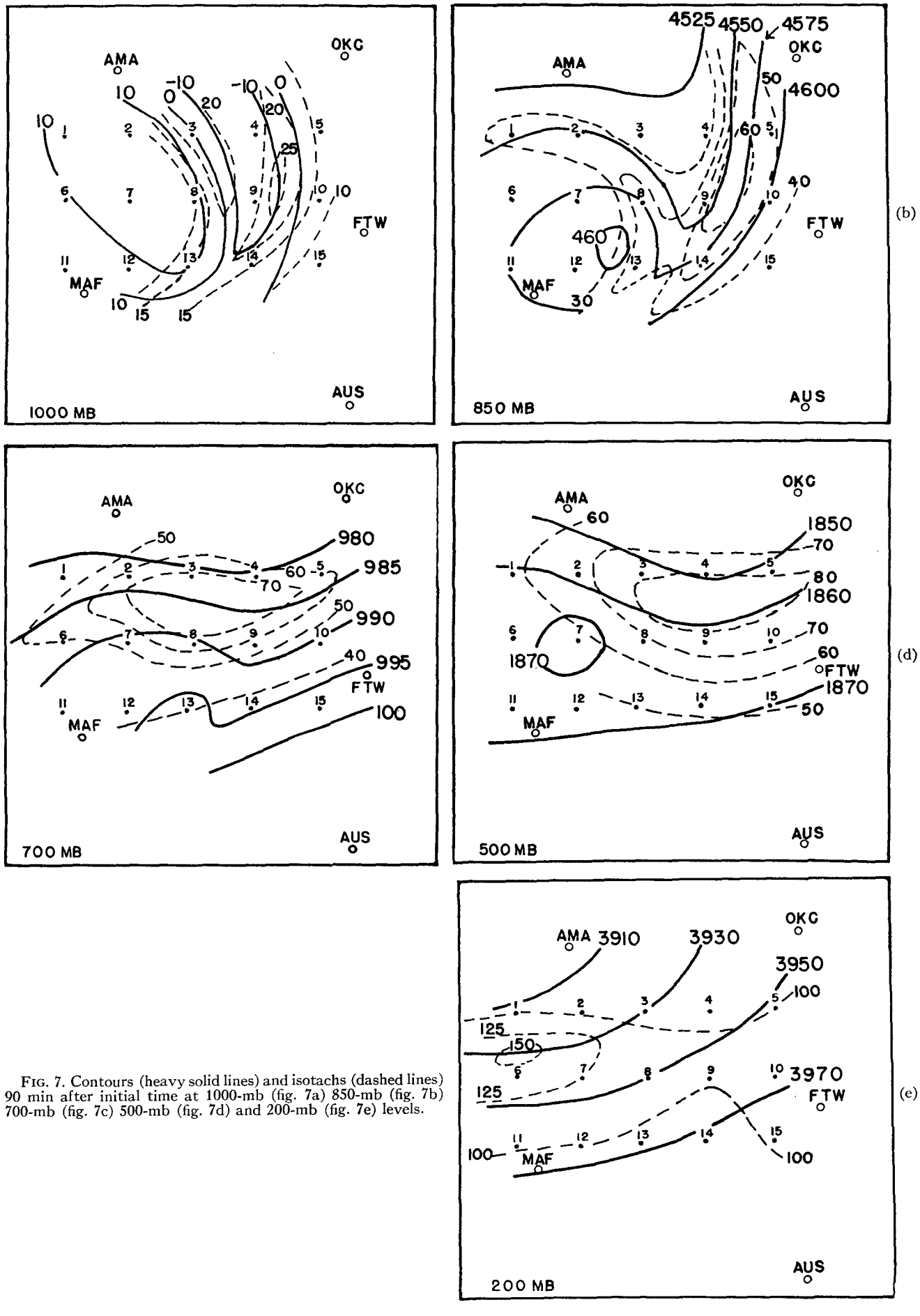

FIG. 7. Contours (heavy solid lines) and isotachs (dashed lines) 90 min after initial time at 1000-mb (fig. 7a) 850-mb (fig. 7b) 700-mb (fig. 7c) 500-mb (fig. 7d) and 200-mb (fig. 7e) levels.

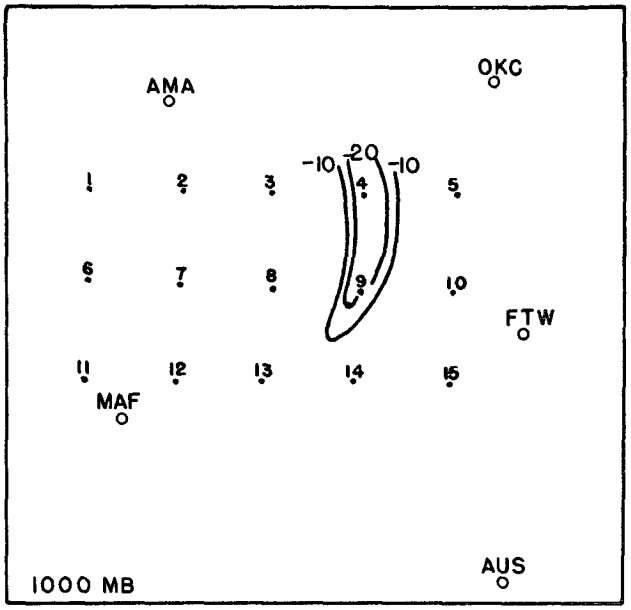

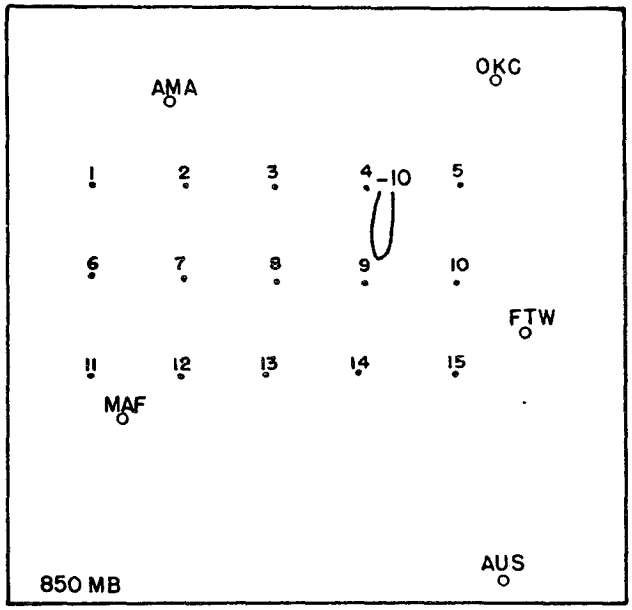

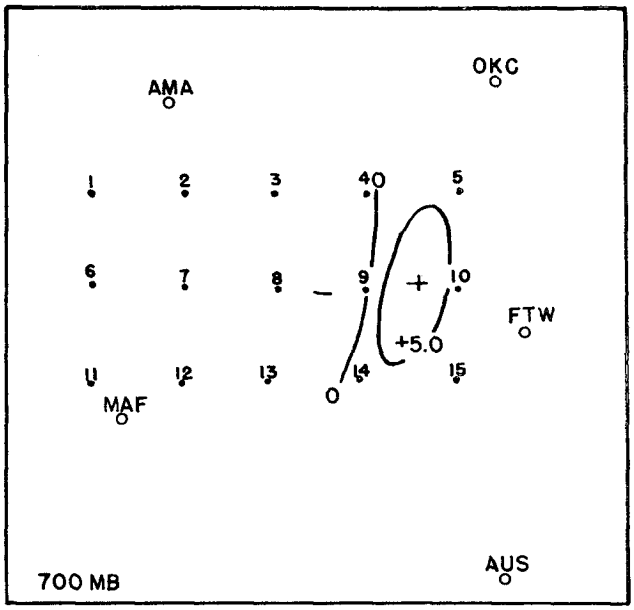

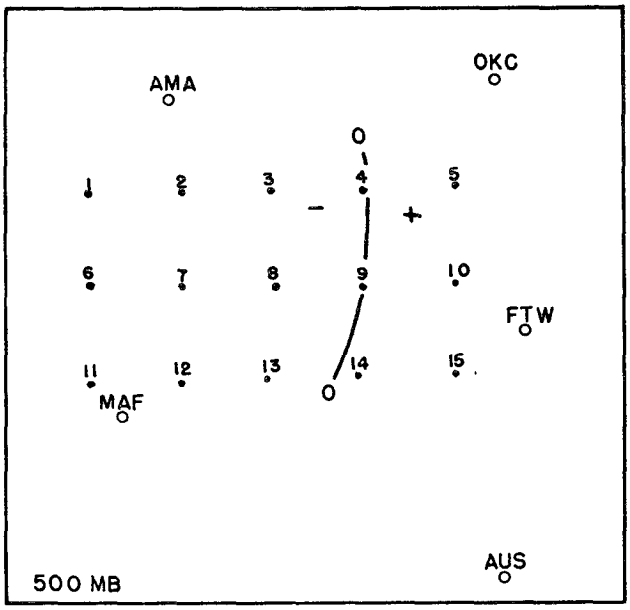

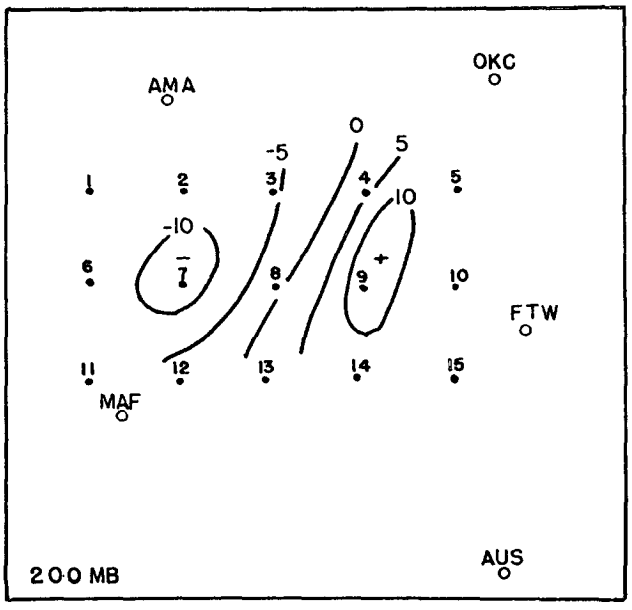

FIG. 8. Distribution of $\mathrm{div}_2 \mathbf{V}$ of fig. 7 (initial time plus 90 min) at levels indicated in units of 10^{-5} sec^{-1}. Positive values: divergence; negative values: convergence.

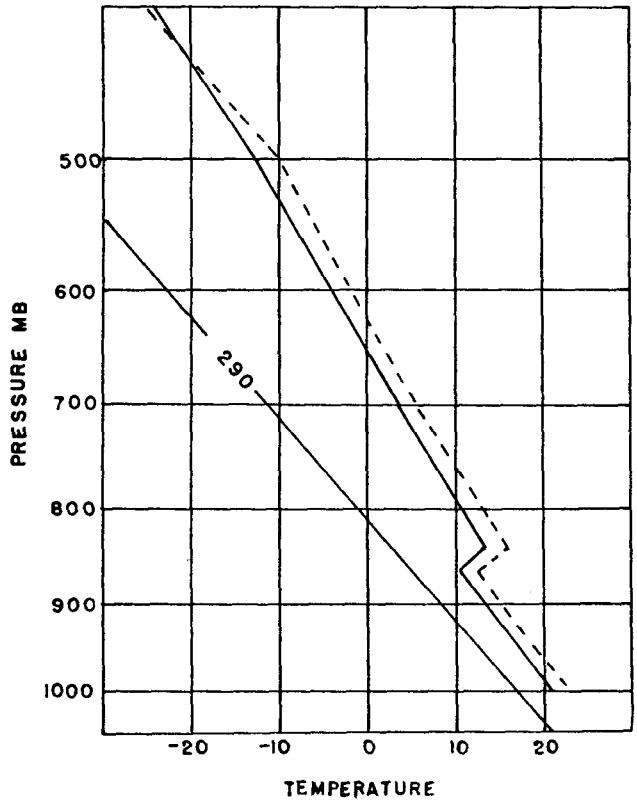
PRESSURE MB
500
600
700
800
900
1000
290
-20
-10
0
10
20
TEMPERATURE

(a)

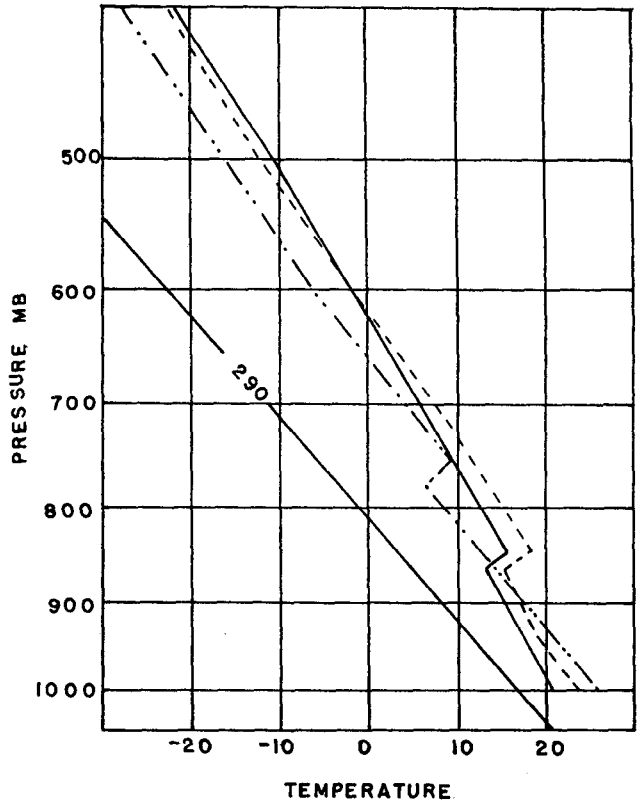
PRESSURE MB
500
600
700
800
900
1000
290
-20
-10
0
10
20
TEMPERATURE

(b)

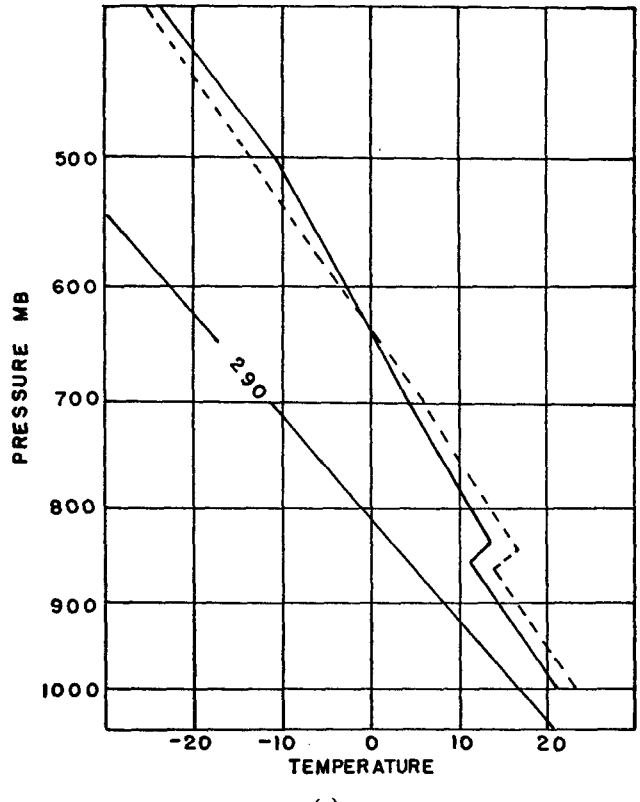
PRESSURE MB
500
600
700
800
900
1000
290
-20
-10
0
10
20
TEMPERATURE

(c)

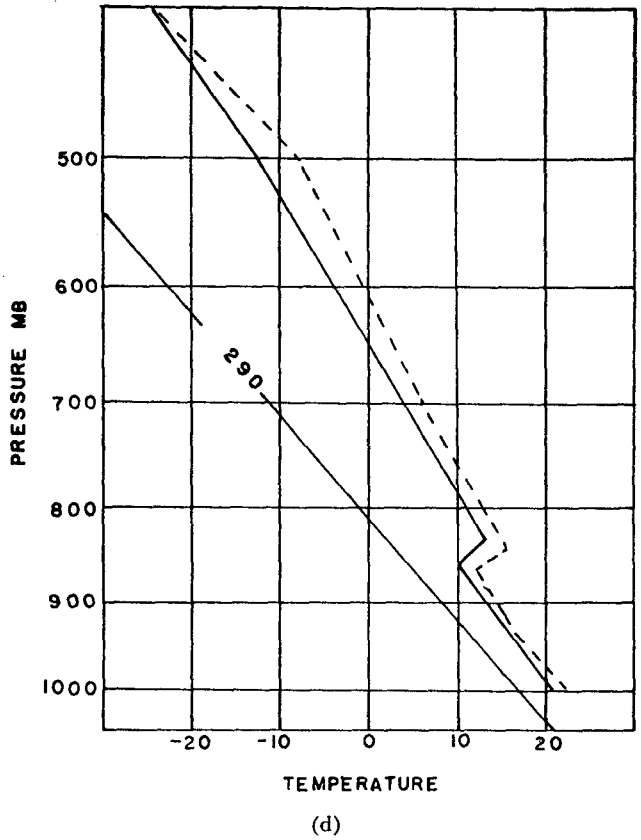
PRESSURE MB
500
600
700
800
900
1000
290
-20
-10
0
10
20
TEMPERATURE

(d)

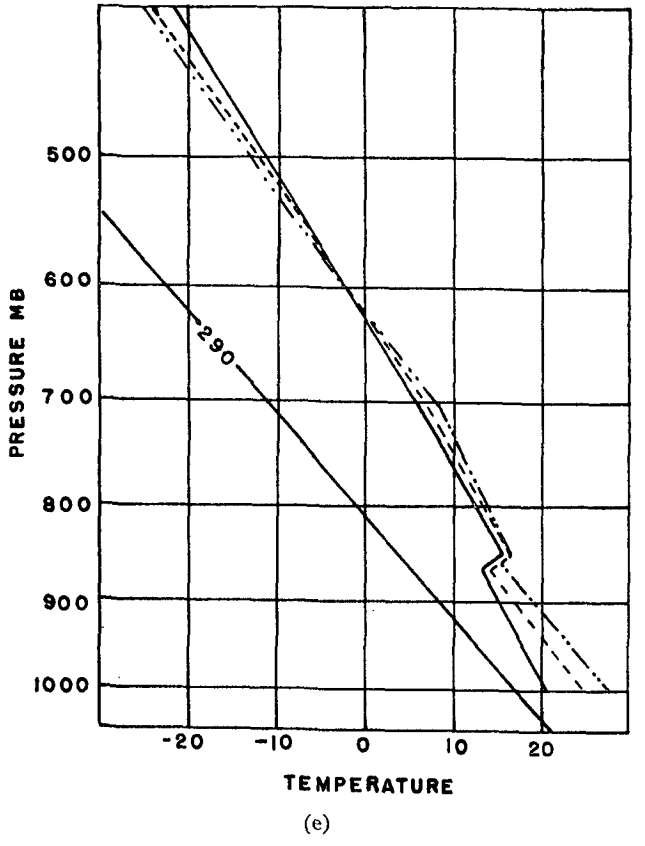

(e)

FIG. 9. Temperature soundings over points 6 (fig. 9a), 7 (fig. 9b), 8 (fig. 9c), 9 (fig. 9d) and 10 (fig. 9e). Heavy solid lines represent temperature at initial time. Dashed lines represent temperature computed 90 min over initial time, and dash-dot and dot lines represent temperature two hours and thirty minutes after initial time.

adiabatic heat interchange were permitted to act for 60 min on the temperature sounding over points 4, 5, 9, 10, 14, and 15. As at the end of the first time step, values of mean temperature and the thicknesses of the several layers were determined. Soundings consistent with these data were computed for the grid points and those for points 9 and 10 are shown in figs. 9d and 9e. Note that at point 10 the effect of temperature changes is to decrease the magnitude of the inversion mainly because of the effect of low-level insolational heating. At point 9, the horizontal temperature advection has been reduced to zero. Insolational heating has increased the mean temperature of the sounding below 850 mb while vertical motion has resulted in cooling the sounding above 850 mb. To maintain consistency between the mean temperature and thickness of the several layers, the inversion had to be lifted. The amount of lift, 100 mb in one hour, is equivalent to a vertical motion of 28 cm sec^{-1}. This is consistent with the mean vertical velocity of 25 cm sec^{-1} computed for the 850- to 700-mb layer over point 9 and utilized in computing the temperature change (−4.5C) due to vertical motion.

The dash-dot line of fig. 9d, the computed temperature curve at point 9 after 2 hr and 30 min, shows a dry adiabatic lapse rate from the ground up to the 770-mb level. Note that the temperature inversion which was located at the 850-mb level over point 9 at the initial time, as well as 90 min later, has now been lifted to near the 770-mb level, decreasing markedly low-level parcel stability. For example, saturation at the 850-mb level would result in a "Showalter Index" [12] of minus 8 and an LFC of 850 mb. At the initial time, saturation at the 850-mb level would have shown a "Showalter Index" of minus one and an LFC of 700 mb.

In the area to the east of point 9, a combination of the three terms of (1) results in warming of the air mass below the 850-mb level. Likewise, in the layer 850 to 700 mb in the area to the east of point 9, warming occurs with the net result being to maintain the inversion at the 850-mb level as shown in fig. 9e.

As indicated previously, a quantitative evaluation at grid points to the west of point 9 is not reliable due to the meso-scale high and suspected ageostrophic conditions in the vicinity of point 7 at the 500-mb level. However, a qualitative evaluation of horizontal and vertical temperature advection in the several layers of the air mass to the west of point 9 can be made. Warming due to vertical motion should continue quite strong over point 7 in view of the strong convergence center at the 200-mb level. Temperature changes due to vertical motion over point 8 may be relatively small in view of the weak divergence patterns indicated in that vicinity. On the other hand, consideration of wind-direction changes indicates cold horizontal-temperature advection in the layers 1000 to 850 mb and 850 to 700 mb, and warm advection is indicated in the layers above 700 mb in the area immediately to the west of the point 9. Qualitatively, then, we can say that the trend is toward stability immediately to the west of point 9.

Since essentially the same temperature changes have taken place along the trough line to the north and south of point 9, at least up to a distance of the order of 100 mi, the evident result is a band of high instability along the trough line through point 9.

The band of high instability extending through point 9 should, therefore, be relatively narrow, and it is in an area characterized by strong low-level convergence (and positive vertical motion). However, the purpose of this study was to show that there are processes inherent in the observed wind field sufficient to cause decreasing stability in the required region at a fairly rapid rate and before condensation begins and not necessarily to show that the region of decreasing stability is, for example, as narrow as the width of an individual squall line.

A region (at least a narrow band) of decreasing stability is normally a *necessary* but not sufficient condition for formation of a squall line. The most obvious additional requirements are an available low-level moisture supply and low-level convergence. In the plains region of the United States, the required moisture is likely to be available in ample quantity at lower levels along the low-level "jet" depicted in figs. 7a and 7b, at the eastern edge of the chart. The moisture "tongue" extends from some distance either side of the low-level "jet," say westward to point 8 along section 6–10 but probably not further westward in sufficient quantity. The axis of maximum moisture is likely to be along or close to the low-level "jet" and decreases rapidly on the westward side. Therefore, there is some line along the westward edge of the moisture tongue, roughly north-south through point 9, where combined decrease of lapse rate and existing amount of available low-level moisture first results in conditions sufficient for convective storms and therefore formation of a squall line.

The attempt here has been to outline the principal physical process only up to the instant when condensation begins. The further process of squall-line maintenance and propagation involves more complicated factors. It is known, for example, that in addition to the upward motion of warm, moist air in convective cells, there is strong downward motion of rain-cooled air, both processes involving energy of buoyancy that is increased by condensation and precipitation.

4. Discussion of the model

There is insufficient aerological data to prove that all details of the model presented here are exactly as assumed. However, experience and studies indicate strongly that it is realistic.

Instability lines are known to occur most often in the warm sectors of certain types of extratropical cyclones. It is also observed that these lines tend to develop their maximum intensity just prior to or at the time the cyclone also reaches its maximum intensity. Petterssen [10] has shown that a feature of cyclone development is the more rapid movement of an upper trough as compared to the movement of the corresponding lower trough. The cyclonic development takes place over a period of perhaps one or two days, whereas the process described in this paper covers developments over a period of only a few hours. However, as a prelude to discussion of the model or the mechanism of instability-line development, it is of interest to point out that inherent in the steepening of the trough-line slope with height as required for cyclone development, there are certain changes in the three-dimensional temperature field consistent with those associated with instability-line development.

It is evident from hydrostatic considerations that once the trough line position at successive heights becomes vertical the horizontal temperature gradient must be zero at the trough line in the direction normal to the line. It follows then that horizontal temperature advection at the trough line must be zero.

For a normally oriented trough, there is initially cold air to the west of it and warm air to the east. For the trough-line slope to approach the vertical, or become steeper, there must be warming (or greater warming) to the west or cooling (or greater cooling) to the east of the trough line when the low-level trough is not changing intensity. It is known from synoptic observation that prior to instability-line formation some cooling aloft is often observed above the low-level trough and even farther eastward. In the hypothetical data used here to develop the model, initial conditions were chosen such that a low-level trough was not in existence. However, the temperature changes inherent in the assumed initial conditions were such that a trough with vertical slope developed in a short time period between the 1000-mb and 500-mb levels.

The fact that relatively greater cooling takes place aloft, as compared to the lower levels, in the region of an instability line according to the model presented here (see points 4 and 9 of table 1 and 2) is consistent with Lloyd's postulation [8] of an upper cold front as a factor in causing tornadoes. However, present thinking does not require an identifiable upper cold front to exist. Fulks [5] postulated that differential cooling with height caused by differential horizontal advection is an important factor in formation of the instability line. However, it needs to be emphasized that under certain conditions of *horizontal temperature advection and vertical motion* the net change can be towards increased stability in the lower layers. See, for example, the temperature changes at the 2.25-km and 4.25-km levels of points 1, 2, and 6 of table 1. Therefore, the forecaster needs to ascertain that differential cooling with height as a consequence of differential horizontal temperature advection is not being offset by temperature changes due to vertical motion.

Beebe and Bates [2] pointed out the significance of 500-mb "jets" crossing 850-mb "jets" as a factor which assists in, or possibly in some cases effects, the release of convective instability through vertical stretching or lifting. The initial wind patterns postulated in the process described here are consistent with those presented by Beebe and Bates.

Fujita [6] in some meso-analyses computed values of surface horizontal-velocity convergence as high as

30×10^{-5} sec^{-1} at the leading edge of the instability line and values of surface horizontal-velocity divergence of at least twice that amount to the rear of the leading edge of the line. In the case at hand, values of surface low-level convergence were computed to be in excess of 20×10^{-5} sec^{-1} at the end of the first time period. Although divergence computations were not made to the west of point 9, the existence of the high-pressure area indicates divergence at the surface. Similarity to the Fujita analyses exists in spite of the fact that his computations were made from data taken at the time convective activity was in progress.

In a synoptic approach to the instability-line problem, Whiting [13] showed by empirical evidence that the beginning of squall-line activity is related to the average east-west separation of the low-level trough and the corresponding 500-mb trough, as would be required by the mechanism discussed in this paper.

A recent synoptic study by Porter and others [11] showed that the pre-cold-frontal-type squall line forms 150 to 250 mi east of a marked cyclonic bend in the jet stream. They also found that, with this type, the squall line tends to form when a jet maximum is coming around the southeast portion of the trough into a delta zone just east of the line or area of greatest cyclonic curvature in the jet stream. These features are in accord with the conditions assumed and computed in this paper. The mechanism seems to be in accord also with other types discussed by Porter and associates.

In a study of squall-line formation in the southeastern United States, Crawford [3] reasons that warm advection and rising contours at 700 and 500 mb to the northwest of the 700-mb cold tongue may intensify the 700-mb trough and thus cause the contours to become more nearly perpendicular to the cold tongue. This increased cold advection augments the instability-line development. This would be in accord with the temperature changes required in the steepening of the slope of the trough line with height and is not inconsistent with the model postulated here.

Fawbush and Miller [4] pointed out that a narrow band of strong winds exists in the middle troposphere prior to tornado occurrence. They argued that this strong wind, which is normally dry, is diverted downward by precipitation to maintain low-level convergence along the instability line. Harrison and Orendorff [7] earlier suggested that a pseudo cold front exists along a non-frontal squall line because of rain-cooled air, and that this is a factor in maintaining the squall line. These factors can operate only after precipitation begins and, while they may be important factors in maintaining the activity, the occurrence of precipitation does not seem to be a necessity in the production of an instability line.

5. Conclusions

From the theoretical considerations presented here which find support in empirically derived procedures and synoptic studies, the problem of forecasting the formation of certain types of instability lines can proceed mainly by the use of indirect evidence of the mechanism in action. Indications are that "precision forecasting" of this phenomena must await a more dense network of upper-air sounding stations and perhaps the utilization of machine methods in processing the data. However, some improvement in manual methods of forecasting the phenomena can be expected as a result of the mechanism proposed here through the proper evaluation and interfunctioning of the horizontal temperature advection and vertical-motion processes as well as various other parameters now in general use.

6. Further research

Although empirical procedures and synoptic studies tend to support the existence of the mechanism, it remains to be established by supporting observational evidence the extent to which the model described here actually plays in the formation of instability lines. A closer network of observations both in space and time is necessary for that purpose.

Much research needs to be done on synoptic methods of detection and forecasting of the movement of minor troughs aloft that synoptic experience has shown to be important to the forecasting of the instability-line phenomena.

Acknowledgment.—The author gratefully acknowledges the advice and counsel of Messrs. C. F. Van Thullenar, J. R. Fulks, L. A. Hughes, and D. T. Williams and their many helpful suggestions in pursuing the study.

REFERENCES

1. Beebe, R. G., 1956: Tornado composite charts. *Mon. Wea. Rev.*, **84**, 127–142.
2. Beebe, R. G., and F. C. Bates, 1955: A mechanism for assisting in the release of convective instability. *Mon. Wea. Rev.*, **83**, 1–10.
3. Crawford, M. E., 1950: A synoptic study of instability lines. *Bull. Amer. meteor. Soc.*, **31**, 351–357.
4. Fawbush, E. J., R. C. Miller, and L. G. Starrett, 1951: An empirical method of forecasting tornado development. *Bull. Amer. meteor. Soc.*, **32**, 1–9.

5. Fulks, J. R., 1951: The instability line. *Compendium Meteor.*, Boston, Amer. meteor. Soc., 647–652.
6. Fujita, T., 1955: Results of detailed synoptic studies of squall lines. *Tellus*, **7**, 405–436.
7. Harrison, H. T., and W. K. Orendorff, 1941: *Pre-cold frontal squall lines*. United Air Lines Meteor. Dept. Circ. No. 16.
8. Lloyd, J. R., 1942: The development and trajectories of tornadoes. *Mon. Wea. Rev.*, **70**, 65–75.
9. Panofsky, H., 1956: *Introduction to dynamic meteorology*. University Park, Penn., Penn. State Univ., pp. 35–36, 101–102, and 125.
10. Petterssen, S., 1956: *Weather analysis and forecasting*, Vol. 1, 2nd ed. New York, McGraw-Hill, pp. 351.
11. Porter, J. M., L. L. Means, J. E. Hovde, and W. B. Chappell, 1955: A synoptic study of squall lines in the North Central United States. *Bull. Amer. meteor. Soc.*, **36**, 390–396.
12. Showalter, A. K., 1953: A stability index for thunderstorm forecasting. *Bull. Amer. meteor. Soc.*, **34**, 250–252.
13. Whiting, R. M., 1954: *A synoptic approach to the trigger mechanism of pre-frontal line squalls*. Eastern Air Lines Sci. Rep. No. 2, 73–88.